Role of Tropical Variability in Driving Decadal Shifts in the Southern Hemisphere Summertime Eddy-Driven Jet

DONGXIA YANG,[a] JULIE M. ARBLASTER,[a,b] GERALD A. MEEHL,[b] MATTHEW H. ENGLAND,[c] EUN-PA LIM,[d] SUSAN BATES,[b] AND NAN ROSENBLOOM[b]

[a] *ARC Centre of Excellence for Climate Extremes, Monash University, Clayton, Victoria, Australia*
[b] *National Center for Atmospheric Research, Boulder, Colorado*
[c] *ARC Centre of Excellence for Climate Extremes, Climate Change Research Centre, University of New South Wales, Sydney, New South Wales, Australia*
[d] *Bureau of Meteorology, Melbourne, Victoria, Australia*

(Manuscript received 8 August 2019, in final form 4 April 2020)

ABSTRACT

The Southern Hemisphere summertime eddy-driven jet and storm tracks have shifted poleward over the recent few decades. In previous studies, explanations have mainly stressed the influence of external forcing in driving this trend. Here we examine the role of internal tropical SST variability in controlling the austral summer jet's poleward migration, with a focus on interdecadal time scales. The role of external forcing and internal variability are isolated by using a hierarchy of Community Earth System Model version 1 (CESM1) simulations, including the pre-industrial control, large ensemble, and pacemaker runs. Model simulations suggest that in the early twenty-first century, both external forcing and internal tropical Pacific SST variability are important in driving a positive southern annular mode (SAM) phase and a poleward migration of the eddy-driven jet. Tropical Pacific SST variability, associated with the negative phase of the interdecadal Pacific oscillation (IPO), acts to shift the jet poleward over the southern Indian and southwestern Pacific Oceans and intensify the jet in the southeastern Pacific basin, while external forcing drives a significant poleward jet shift in the South Atlantic basin. In response to both external forcing and decadal Pacific SST variability, the transient eddy momentum flux convergence belt in the middle latitudes experiences a poleward migration due to the enhanced meridional temperature gradient, leading to a zonally symmetric southward migration of the eddy-driven jet. This mechanism distinguishes the influence of the IPO on the midlatitude circulation from the dynamical impact of ENSO, with the latter mainly promoting the subtropical wave-breaking critical latitude poleward and pushing the midlatitude jet to higher latitudes.

1. Introduction

As the leading mode of atmospheric variability in the Southern Hemisphere (SH) extratropics, the southern annular mode (SAM) and its associated eddy-driven jet (or midlatitude jet) are fundamentally important for the climate system. The SAM has been shown to have well-established connections with SH subtropical and extratropical rainfall bands (Purich et al. 2013; Hendon et al. 2014; Lim et al. 2016a). Consequently, a range of observational and model studies have sought to understand the observed poleward movement of the eddy-driven circulation in the SH over recent decades.

A poleward shift of the SH eddy-driven circulation under increasing greenhouse gases and stratospheric ozone depletion has been emphasized in early studies (Kushner et al. 2001; Yin 2005). Thompson and Solomon (2002) highlighted the contribution of stratospheric ozone depletion to a positive SAM trend, especially over the SH summertime since the 1960s, based on multiple observed datasets from 1969 to 1998. Arblaster and Meehl (2006) further classified different sources of external forcings and their contributions to the SAM trend using a global coupled model and indicated that the ozone changes in the upper troposphere and stratosphere dominated the observed positive SAM trend. Similar results were obtained by Polvani et al. (2011), who found that the impact of ozone depletion was 2–3 times larger than GHGs on the summertime poleward displacement of the eddy-driven jet and the expansion of the Hadley cell over the second half of the twentieth century.

Corresponding author: Dongxia Yang, dongxia.yang@monash.edu

DOI: 10.1175/JCLI-D-19-0604.1

The contributions of natural intrinsic variability, particularly the influence of tropical sea surface temperatures (SSTs), have also been discussed, with a primary focus on interannual time scales. A number of previous studies have shown an association between El Niño–Southern Oscillation (ENSO) and a SAM phase shift via zonally symmetric variations in transient eddy momentum flux anomalies (L'Heureux and Thompson 2006; Fogt et al. 2011; Gong et al. 2013; Yu et al. 2015). During La Niña events, a positive SAM phase occurs more frequently and the opposite is found for El Niño years. Chen et al. (2008) further analyzed the eddy momentum flux spectrum and found that the midlatitude jet could be expected to undergo a poleward migration during La Niña years due to the poleward displacement of the wave-breaking critical latitude—and of the associated transient eddy momentum flux divergence and convergence zones, by waves of a broad range of phase speeds.

Despite the well-established interannual ENSO–SAM relationship, less is known about the influence of internal decadal variability on the midlatitude jet. Some research has related the interdecadal Pacific oscillation (IPO) transition in the late 1990s to Antarctic climate variability. For example, the negative phase of the IPO has been linked to Antarctic sea ice expansion via a positive phase of the SAM combined with a deepened Amundsen Sea low (ASL), which alters the wind patterns over the Antarctic sea ice zone (Meehl et al. 2016; Purich et al. 2016; Clem et al. 2019; Holland et al. 2019; Meehl et al. 2019b). Recent studies have also highlighted the role of Atlantic and Indian Ocean SSTs on Antarctic climate. For instance, Li et al. (2015) suggested that tropical Atlantic SSTs could force a positive response in the SAM and a strengthened ASL via stationary Rossby wave activities in SH winter. Wang et al. (2019) and Purich and England (2019) found that tropical Indian Ocean SST likely contributed to the Antarctic sea ice decline in austral spring 2016 via SAM and zonal-wave-3 (ZW3) teleconnections.

A few studies have further distinguished the relative roles of radiative forcing and global SST on SH midlatitude jet variations. For example, Lee and Feldstein (2013) applied a cluster analysis based on ERA-Interim data and concluded that ozone contributed about 50% more than GHG toward the SH summertime jet shift from 1979 to 2008, with tropical convection playing an important role for the GHG-driven trend. Similar results were obtained in other studies examining simulations with time-evolving SST and external forcing prescribed in atmosphere-only models. For instance, Deser and Phillips (2009) emphasized the importance of radiative changes as the dominant driver of the poleward movement of the SH westerly jet in austral summer [December–February (DJF)] during 1951–2000 using Community Atmosphere Model version 3 (CAM3) experiments. Schneider et al. (2015) suggested that ozone depletion could largely explain the positive SAM pattern during 1979–2011 in the austral summer season, while teleconnections from tropical SSTs also play a role, indicating that the extratropical circulation responds to a combination of both (external) radiative forcing and (internal) tropical SST variability. However, there remain issues with using atmosphere-only experiments to study the combined effects of external radiative forcing and internal SST variability. First, compared to coupled models, atmosphere-only experiments lack the interactions with the underlying ocean and sea ice, which could be important for tropical–extratropical teleconnections. Second, the time-evolving global SSTs still implicitly contain the GHG-induced forced response, which makes it difficult to delineate between the influence of external forcing and the influence of internal variability in SST.

Here we examine the separate roles of internally driven tropical SSTs and external forcing in the observed decadal variability of SH midlatitude circulation using the CESM1(CAM5) coupled model large ensemble (Kay et al. 2015) as well as various pacemaker experiments. We will address the following overarching questions:

1) What are the relative roles of external forcing versus internally driven SST variability in the tropical Pacific, tropical Indian, and tropical and North Atlantic Ocean basins in recent decadal variations of the SH summertime midlatitude circulation?
2) By what mechanism does the SH summertime eddy-driven jet respond to tropical Pacific SST on decadal time scales?

We focus on the austral summer season since that has experienced the strongest observed latitudinal shift over the satellite era (Swart et al. 2015; Lim et al. 2016b), for which we have the most reliable data. Furthermore, there has been much research undertaken regarding the influence of external forcings on the SH atmospheric circulation shift in this season, but very little work on the impact of internal variability on decadal time scales. The rest of this paper is organized as follows: Section 2 describes the data, the model simulations, and the methodology employed in this study. Section 3 presents the main results. The physical mechanisms at play are outlined in section 4, and a summary with discussion is given in section 5.

TABLE 1. Summary of the CESM1.1 simulations used in this research. All experiments begin in January 1920 and extend until the end of December 2013, apart from the PI control run, where years 400–2100 are selected.

Experiments	Time-evolving external forcing	Time-evolving SSTs	Members
Preindustrial control (PI control)	1850 conditions, years 400–2100	—	1
Large Ensemble (LENS)	Historical for 1920–2005, RCP8.5 for 2006–13	—	40
Pacific pacemaker	As in LENS, except with SPARC ozone forcing	Fully restored SSTA for 15°S–15°N, buffer belts for 15°–20°S and 15°–20°N, 180° to the American coast	10
Indian pacemaker	As in LENS, except with SPARC ozone forcing	Fully restored SSTA for 15°S–15°N, buffer belts for 15°–20°S and 15°–20°N, from the African coast to 180°	10
Atlantic pacemaker	As in LENS, except with SPARC ozone forcing	Fully restored SSTA for 5°–55°N, buffer belts for 0°–5°N and 55°–60°N, the Atlantic basin	10

2. Data and methods

Our study is primarily confined to the DJF season during the 1979–2013 period due to the availability of both reliable observational data and output from the CESM pacemaker simulations.

a. Reanalysis data

Zonal (U) and meridional (V) winds and mean sea level pressure (MSLP) from January 1979 to February 2013 are taken from the European Centre for Medium-Range Weather Forecasts interim reanalysis (ERA-Interim; Dee et al. 2011). The observed monthly SST over the global oceans between January 1870 and December 2013 is taken from the Hadley Centre HadISST1 dataset (Rayner et al. 2003).

b. The Community Earth System Model simulations

Climate variations are caused by both external radiative forcing and internal variability. The latter arises from the internal processes of each climate component (atmosphere, ocean, land, cryosphere, etc.), as well as their coupled interactions. To separate the internal variability and the influence of the external forcing, five sets of Community Earth System Model version 1.1 (CESM1.1) experiments are analyzed in this paper (Table 1). The CESM1.1 is a coupled Earth system model consisting of atmosphere, ocean, land, and sea ice components with a nominal horizontal resolution of 1° (Hurrell et al. 2013; Kay et al. 2015) and contributed to phase 5 of the Coupled Model Intercomparison Project (CMIP5).

The first experiment comprises monthly data from a preindustrial control run (length ≥ 1000 years) with a constant forcing based on 1850 levels (Kay et al. 2015). In the absence of changes in natural or anthropogenic forcing, the fluctuation range in the PI control describes internally generated variability.

The second experiment is the CESM Large Ensemble (LENS), which includes 40 individual members (Kay et al. 2015). All ensemble members of the LENS follow the same radiative forcing scenario (Taylor et al. 2012), with historical forcing during 1920–2005, followed by the high-emission forcing scenario of representative concentration pathway (RCP) 8.5 (Moss et al. 2010) from 2006 to 2080. Ensemble members of the CESM LENS are generated with a small perturbation of the initial atmospheric temperature fields. As a result of the chaotic nature of the climate system, the small initial perturbations evolve into a diverse member spread, which reflects the internally generated variability of the climate system in the presence of external forcing. The LENS 40-member ensemble mean yields an average that removes internal variability and thus gives an estimate of the influence of external forcing on the climate system. It is noted that the LENS members have very different tropical trends (Chung et al. 2019); thus, to best estimate the external forcing signal and to be comparable with previous work using LENS (Solomon and Polvani 2016; Holland et al. 2019; Zhang et al. 2019), we employed 40 members of the LENS throughout our study.

The remaining experiments use a pacemaker framework (Kosaka and Xie 2013; Schneider and Deser 2017; Meehl et al. 2019a), wherein SST anomalies (SSTA) are nudged to observed values within a specific ocean region, while the rest of the model evolves freely. In all pacemaker experiments (Table 1), the identical coupled model and external forcing used in the LENS is employed, aside from ozone forcing, wherein the LENS employs the Whole Atmosphere Community Climate Model (WACCM; Marsh et al. 2013) ozone dataset, while the pacemaker runs are forced with the Stratosphere–Troposphere Processes and their Role in Climate (SPARC) stratospheric ozone data (Cionni et al. 2011). In these pacemaker experiments, SSTA are nudged to

the NOAA Extended Reconstruction Sea Surface Temperature version 3b (Smith et al. 2008) observed anomalies, with a climatological period of 1920–2005. For example, in the CESM tropical Pacific Ocean pacemaker run (Table 1), a fully restored observational SSTA was applied over the region 15°S–15°N, 180° to the American coast, with two buffer belts along 15°–20°S and 15°–20°N. In these buffer zones, the fully nudged SSTA (at 15°S and 15°N) are gradually damped to zero (at 20°S and 20°N) via a sine function of the latitude change (Schneider and Deser 2017). The rest of the model is fully coupled and free to evolve, and able to capture the response to both external forcing and the observed SST changes in this specified region. Following the method of Schneider and Deser (2017) and Holland et al. (2019), the ensemble mean of the Pacific pacemaker combines the response to external forcing and the response to observed tropical Pacific SSTs, and thus removing the ensemble mean of the LENS gives an estimate of the response of the global climate system to observed time-varying internally driven Pacific SSTs. Note that while the ozone forcing differs slightly between the LENS and the pacemaker experiments, Schneider and Deser (2017) concluded that the ozone forcing differences had statistically indistinguishable impacts on the trends in the SH eddy-driven jet over the satellite era. Given the LENS stratospheric ozone forcing (WACCM) has stronger ozone depletion over that period than the SPARC ozone forcing (Cionni et al. 2011) used in the pacemaker experiments (Eyring et al. 2013), if anything our methodology for subtracting the externally forced signal would weaken the determined impact of tropical internally generated SSTAs.

A similar methodology is applied to isolate the tropical Indian Ocean (15°S–15°N; African coast to 180°) and tropical and North Atlantic SST (0°–60°N; Atlantic basin) impact in the other pacemaker experiments (Table 1). By subtracting the LENS ensemble mean from the separate pacemaker ensemble means, we obtained the climate response to the internal variability originating from the tropical Pacific SST, tropical Indian Ocean SST, and the northern and tropical Atlantic SST, respectively. The sum of these four components (i.e., LENS, plus the three pacemakers with external forcing removed) reflects the estimated response of the climate system to both external forcing and the internally generated observed variability in the three tropical basin SSTs. However, this linear summation does not take into account tropical basin interactions (Cai et al. 2019) and may result in some ''double counting'' of the influence of tropical SSTs on the extratropical circulation. Finally, note that daily U and V winds are not available for the Indian and Atlantic pacemaker experiments, which limits our exploration of physical mechanisms to the Pacific pacemaker experiment and LENS only.

c. Definitions

1) Eddy-driven jet

The eddy-driven jet is located in the midlatitudes and maintained by an eddy momentum flux convergence (Vallis 2006). Different from the baroclinic thermal-driven subtropical jet, the eddy-driven jet is equivalent barotropic, and the transient eddy–mean flow interaction is important for its development and variation (Hendon et al. 2014). In this paper, the eddy-driven jet is defined as the maximum zonal wind at 850 hPa.

2) Cospectra analysis of transient eddy momentum flux

Cospectra analysis of transient eddy momentum flux ($\overline{u'v'}$) has been widely used to study the changes of midlatitude eddy characteristics (generation, propagation, and dissipation) and their impact on the background zonal flow (Randel and Held 1991; Chen and Held 2007; Chen et al. 2008; Hendon et al. 2014).

Here we calculated the transient eddy momentum flux as a function of eddy phase speed and latitude following Randel and Held (1991). Specifically 1) we obtained the DJF (90 day) daily transient u', v' data from ERA-Interim, CESM LENS, and Pacific pacemaker; 2) at each latitude, we computed the cospectra (real part of the complex cross power spectra) of $\overline{u'v'}$ by Fourier transforming u', v' (longitude, time) to u', v' (wavenumber, frequency), with four passes of Gaussian spectral smoothing [following Eq. (2) in Randel and Held 1991] operating on the frequency dimension; 3) the wavenumber–frequency cospectra were transferred to wavenumber–phase speed cospectra [following Eqs. (3a) and (3b) in Randel and Held 1991]; and 4) we took the summation of zonal wavenumbers 1–10 for plotting the cospectra of $\overline{u'v'}$ as a function of phase speed and latitude. There is some sensitivity to the choice of smoothing method and using monthly versus seasonal length of data, which primarily impacts the low-latitude regions but minimal impacts the midlatitudes where the eddy activity is vigorous.

3) Southern annular mode

The southern annular mode (SAM) is the leading mode of atmospheric variability in the SH extratropics, characterized by a ''see-saw''-like behavior of mass distribution between the mid and high latitudes. In this study, the SAM index is defined as the normalized zonal-mean sea level pressure (SLP) difference between 40°

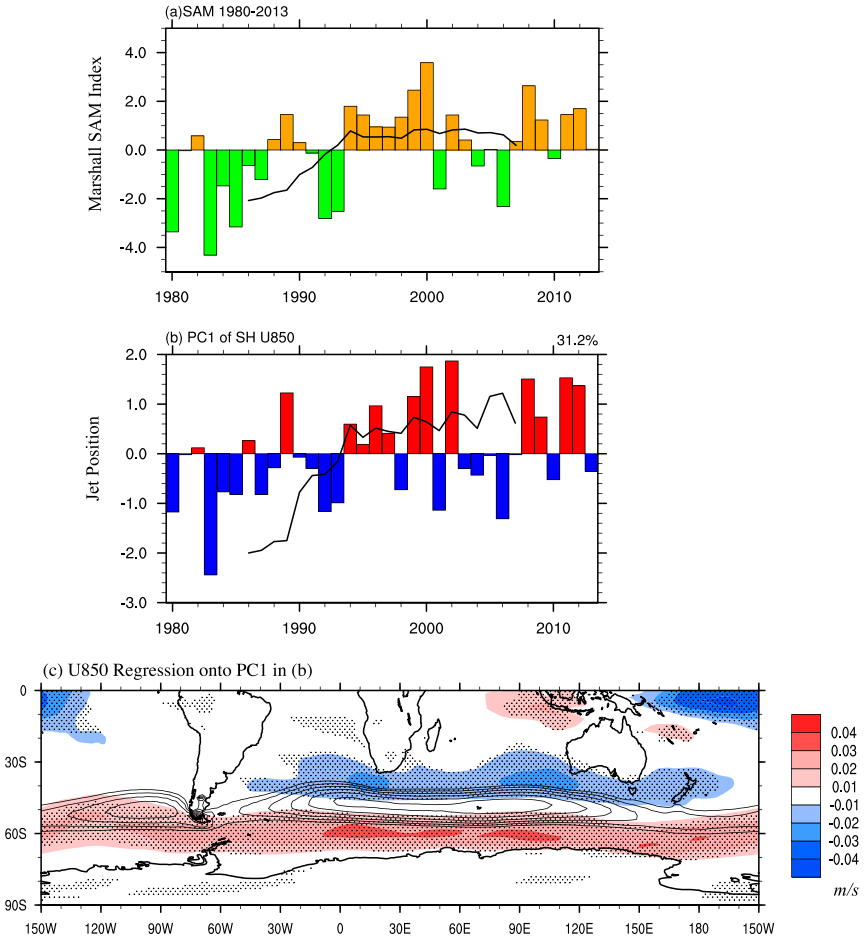

FIG. 1. (a) Marshall SAM time series (bars) for DJF from 1980–2013; the black line is the 11-yr running mean. (b) PC1 time series (bars) of 850 hPa *U* wind during 1980–2013 over 20°–90°S; the black line is the 11-yr running mean. (c) Contours show the climatological midlatitude jet from 1980 to 2013 with an interval of 1 m s^{-1}; colors are the regression of the 850-hPa zonal wind onto the PC1 in (b), with dashed areas significant at the 95% level based on a two-sided Student's *t* test.

and 65°S, following Gong and Wang (1999). A positive SAM phase means higher normalized pressure anomalies over 40°S than over 65°S. This quasi-stationary pattern can be considered as the eddy-driven circulation (Vallis 2006). The SAM phase is associated with the latitudinal location of the eddy-driven jet as well as variations in the jet intensity (Swart and Fyfe 2012; Swart et al. 2015).

4) INTERDECADAL PACIFIC OSCILLATION

The interdecadal Pacific oscillation (IPO) is a representation of internal decadal climate variability in the Pacific Ocean. There are several IPO definitions, and here we use the second principal component (PC2) of the low-pass filtered (13-yr cutoff) near-global SST as in Meehl et al. (2016). A positive IPO phase reflects an eastern Pacific Ocean warming flanked by cooling in the subtropical western Pacific. The negative IPO phase sees SST anomalies of opposite sign to the positive IPO phase.

3. Results

Figure 1 shows the observed SAM variation (Fig. 1a), the leading principal component of the eddy-driven jet (Fig. 1b) and the regression of westerly zonal wind anomalies onto the PC1 time series (Fig. 1c). The peak magnitude of the climatological jet is located in the southern Atlantic and Indian Oceans with maximum wind speeds of around 18 m s^{-1} (see contours in Fig. 1c). The 11-yr running means (lines in Figs. 1a,b) suggest that the SAM gradually trended from a negative to positive phase during 1980–2000 and then plateaued afterward, associated with a poleward shift of the eddy-driven jet

(the dipole structure of anomalies centered on the climatological jet axis in Fig. 1c). As noted above, external forcing is believed to be the dominant driver of the poleward shift in the austral summer eddy-driven jet over the second half of the twentieth century, with ozone depletion being the main contributor (Karpechko et al. 2013). After 2000, Antarctic ozone depletion plateaued (Chipperfield et al. 2017), whereas the IPO transitioned from a positive to negative phase around 1999, as discussed in previous studies (e.g., Meehl et al. 2016) and as shown in Fig. 2. How did the SH midlatitude atmospheric circulation respond to these observed variations in forcing and tropical SSTs?

a. *Decadal difference between 1999–2013 and 1979–98*

To address this question the observed period is divided into two separate periods P1 (1979–98) and P2 (1999–2013) based on the IPO time series in Fig. 2, targeting a comparison between the influence of positive and negative IPO phases, respectively. The significance test of the decadal difference is based on a two-sample *t* test for observation and model ensemble mean. During the positive IPO period (P1), the SAM was primarily in the negative phase, with an equatorward movement (negative PC value in Fig. 1b) of the jet, whereas in the negative IPO period (P2), the SAM was primarily in its positive phase with a poleward displacement of the jet. As discussed earlier, the decadal change of the SAM and the eddy-driven jet cannot be simply inferred as a response to IPO variations, because strong ozone and GHG forcings were also present at this time, along with other tropical ocean SST changes.

Figure 3 shows the decadal difference of sea surface temperature between 1999–2013 and 1979–98 for DJF in observations (Fig. 3a), under the influence of external forcing (Fig. 3c) and from the pacemaker experiments (Figs. 3d–f). To distinguish the influence of external radiative changes from the intrinsic variability due to tropical ocean SSTA, the LENS ensemble mean is subtracted from the CESM pacemaker experiments. In accordance with the IPO time series in Fig. 2, the observed SSTs display a typical negative IPO phase pattern within the Pacific basin, with significant cooling over the central and eastern tropical Pacific, and notable warming over the subtropics. This pattern is only captured in Pacific pacemaker minus LENS (Fig. 3d), which suggests the primary role of internal decadal variability in the observed SST difference, supporting previous work (e.g., England et al. 2014). Meanwhile the impact of external forcing across these two periods warms up the Earth surface almost globally (Fig. 3c). The decadal SST difference due to internally driven tropical and

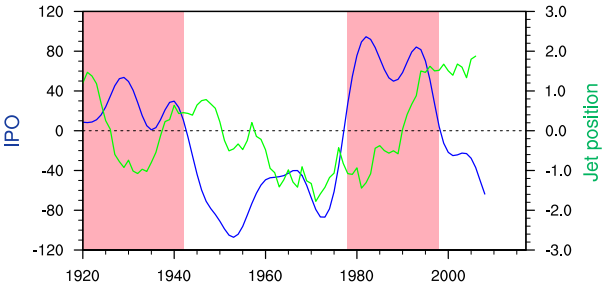

FIG. 2. The smooth blue line is the IPO time series from 1920 to 2013 in DJF calculated as the second EOF of low-pass-filtered (13-yr cutoff) near-global HadISST. Pink bars indicate the positive IPO phase and white bars show the negative phase. The green line is the the 11-yr running mean for the PC1 time series of the 850-hPa zonal wind for 1920–2013 using Twentieth Century Reanalysis (V2) datasets.

North Atlantic SST and tropical Indian Ocean SST are shown in Figs. 3e and 3f, respectively. There is an observed significant warming trend in the North Atlantic, resulting largely from the external forcing and partly from internal variations. However, there are less significant values in the Indian and Atlantic Ocean pacemaker experiments than in the tropical Pacific and from external forcing.

The sum (Fig. 3b) of the external and internal factors (Figs. 3c–f) yields a similar pattern to the observations in most locations except the SH high latitudes, showing that our methodology using the CESM experiments is generally able to separate the different influences and reproduce the observations to a large degree. However, there is too much warming over the Southern Ocean, especially in the southern Atlantic basin and around New Zealand. This could be related to the systematic warm bias of coupled climate models in CMIP5 (Wang et al. 2014), with Kay et al. (2016) identifying insufficient cloud brightness and excessive absorbed shortwave radiation (ASR) biases over the Southern Ocean in CESM1. Second, the equatorial central Pacific SST in Fig. 3b is not cooling enough compared with Fig. 3a, suggesting that the model has problems reproducing the strength of the Pacific trade wind acceleration across this time period. This issue also seems to affect all coupled models and has been touched upon in several past studies, for example (England et al. 2014; McGregor et al. 2014; Luo et al. 2018; McGregor et al. 2018). Furthermore, the North Atlantic pacemaker warming induces a positive IPO-like pattern in the Pacific basin (Fig. 3e), which is opposite to the result obtained by McGregor et al. (2018) and Meehl et al. (2019a). While noting these caveats, the pacemaker experiments remain a useful tool to test and understand the influence of each basin in driving SH circulation changes.

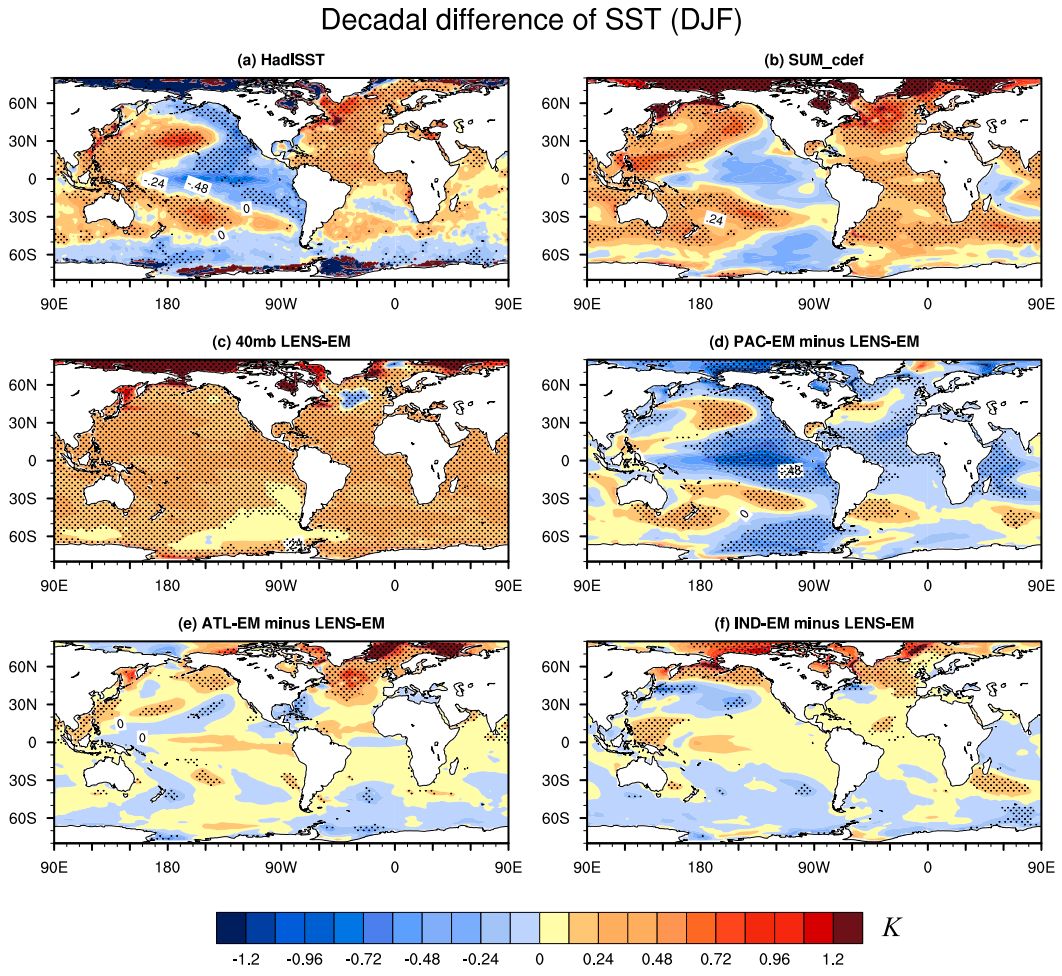

FIG. 3. The decadal difference between averaged P2 (1999–2013) and P1 (1979–98) for sea surface temperature. (a) HadISST; (b) sum of (c)–(f); (c) CESM Large Ensemble mean (LENS-EM), indicative of external forcing; (d) Pacific pacemaker ensemble mean (PAC-EM) minus LENS-EM, highlighting the internally driven tropical Pacific SST impact; (e) Atlantic pacemaker ensemble mean (ATL-EM) minus LENS-EM; and (f) Indian pacemaker ensemble mean (IND-EM) minus LENS-EM. Stippling in (a) and (c)–(f) indicates that differences between the two periods are significant at the 95% level based on a *t* test.

The decadal difference analysis is shown for the austral summer 850-hPa zonal wind in Fig. 4. With easterly wind anomalies in the midlatitudes (north of 45°S) and westerly wind anomalies in the high latitudes (south of 45°S), the dipole structure shows that the observed eddy-driven jet has migrated poleward by ~1° of latitude during 1999–2013 relative to 1979–98 (refer to contours in Fig. 4a). Significant values are found over the South Atlantic and parts of the Indian Ocean basin.

More quantitative features of the jet shift for the zonal mean and each basin average are shown in Fig. 5. The jet position is identified as the latitude of the maximum zonal wind at 850 hPa, which is obtained using a quadratic fit to the grid point with the maximum zonal wind and the eight adjacent to it (Simpson et al. 2018). The 5%–95% confidence intervals (shaded boxes) in Fig. 5 are determined from the spread across the 40- or 10-member ensembles, following Eq. (8) of Swart et al. (2015). The LENS with its larger ensemble size therefore has a narrower confidence interval.

From the zonal-mean perspective, the observed jet movement (triangles in Fig. 5) from 1979–98 to 1999–2013 is ~0.8°S (0.23° decade^{-1}), which is significantly driven by both the external forcings (0.5°S ± 0.18°) and the Pacific SST (0.4°S ± 0.34°) based on our model simulations. This magnitude of the jet movement is consistent with the ~2° (0.3° decade^{-1}) latitudinal shift found by Swart et al. (2015) for DJF over the longer 1951–2011 period, with some difference due to a different mix of forcing and internal variability between the two periods expected. The largest observed jet shift is found in the South Atlantic basin, with ~1.3°S

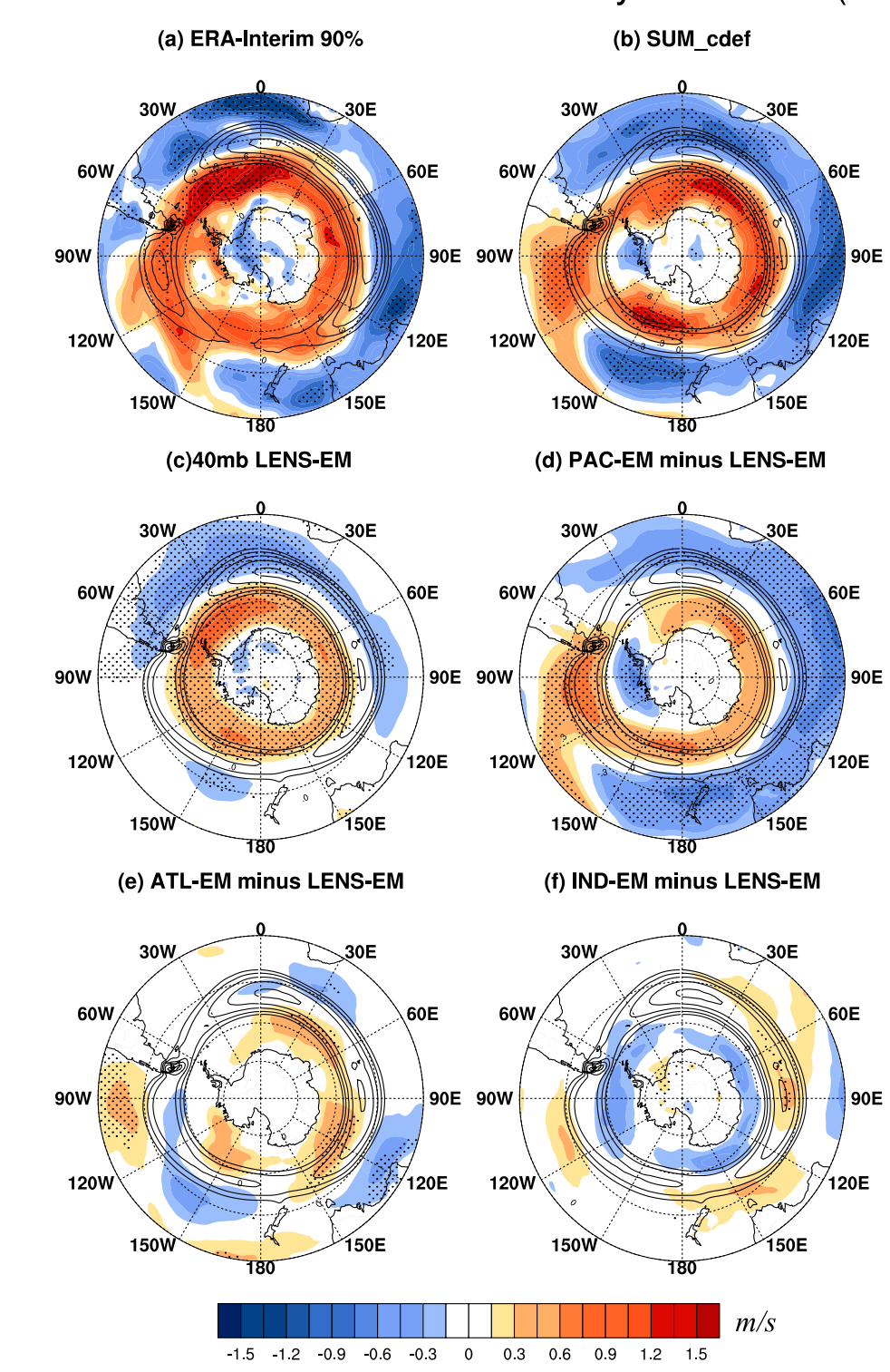

FIG. 4. The decadal difference between averaged P2 (1999–2013) and P1 (1979–98) for 850-hPa zonal wind. (a) ERA-Interim; (b) sum of (c)–(f); (c) LENS-EM; (d) Pacific pacemaker ensemble mean (PAC-EM) minus LENS-EM; (e) Atlantic pacemaker ensemble mean (ATL-EM) minus LENS-EM; and (f) Indian pacemaker ensemble mean (IND-EM) minus LENS-EM. Contours are the 850-hPa zonal wind averaged over P1 using ERA-Interim in (a) and the LENS ensemble mean in (b)–(f). Stippling in (a) and (c)–(f) indicates that differences are significant at the 90% and 95% level based on a *t* test, respectively.

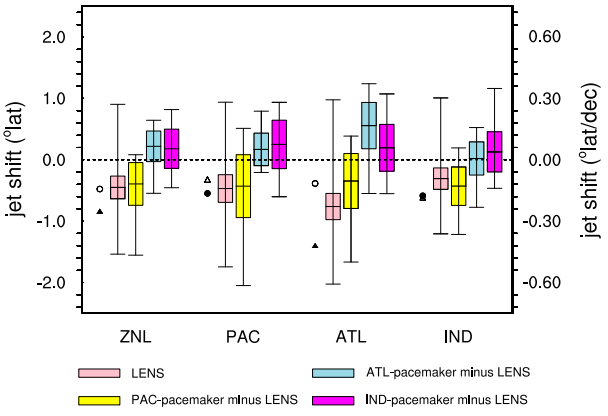

FIG. 5. The decadal difference between averaged P2 (1999–2013) and P1 (1979–98) of 850-hPa jet position for zonal mean and basin averages. Negative values indicate the poleward shift. For each model experiment, the ensemble-mean jet shift is given by the middle horizontal line, the 95% confidence interval is shown as the vertical colored bars, and the minimum and maximum shifts (equivalent to the 2.5th and 97.5th percentiles, respectively) across the ensemble are displayed as the upper and lower whiskers. The model summation of the external forcing and internal variabilities is given by small circles. The jet shift in ERA-Interim is shown as the small triangles. Solid triangles and circles indicate that the decadal difference are significant at the 90% level based on the same *t* test as in Fig. 4. The longitude range for each basin is defined as 150°E–70°W for the South Pacific, 70°W–20°E for the South Atlantic, and 20°–150°E for the southern Indian Ocean basin.

poleward displacement, where external forcing contributed ~0.8°S (±0.21°) and the influence of Pacific SST is ~0.3°S (±0.44°). In the southern Indian Ocean basin, the observed magnitude of the jet shift is around 0.6°S, which is mainly induced by Pacific SST internal variability (~0.4°S ± 0.31°) as well as the external forcing (~0.3°S ± 0.17°). The smallest jet movement in the observations is detected in the South Pacific basin of ~0.3°S, with 1 m s^{-1} acceleration of the maximum wind mainly driven by Pacific SST (see Fig. 4). This is consistent with Schneider et al. (2015), who found that the zonal wind in the South Pacific experienced an intensification with a slight poleward shift (their Fig. 8a) during 1979–2011. It is also clear that the North Atlantic and tropical Atlantic SST (Fig. 4e and blue bars in Fig. 5), as well as the tropical Indian Ocean SST (Fig. 4f and magenta bars in Fig. 5), appear to force a much weaker response, which sometimes can partly offset the poleward trend caused by external forcing and Pacific SST. If we simply add up the externally forced response and the internally generated responses from all three tropical ocean basins (Fig. 4b), all these combined factors are able to reproduce the observed poleward jet migration over the Atlantic and Indian Oceans, as well as the jet strengthening over the southeastern Pacific to some degree, but there are mismatches with some locations of the statistically significant regions.

In summary, based on the results in Figs. 4 and 5, it is evident that the two dominant drivers of the decadal shift in the SH midlatitude jet are external forcing and tropical Pacific SSTAs, with external forcing significantly contributing to the observed poleward jet shift over the South Atlantic basin, while internal tropical Pacific SST variability drives the poleward jet migration in the southern Indian Ocean basin and Pacific basin. This result is consistent with Lee and Feldstein (2013) and Schneider et al. (2015), who found that ozone depletion and teleconnections from tropics-wide SSTs act together to explain the midlatitude poleward jet migration during 1979–2011 in SH summer. Here we further identify that the tropical SST impact is mainly from internally driven variability originating in the tropical Pacific basin.

Consistent results are obtained for the sea level pressure decadal difference, where observations (Fig. 6a) show a zonally symmetric positive SAM phase (negative SLP anomalies at high latitudes, positive SLP anomalies at midlatitudes), with significant changes found mainly in the South Atlantic basin. This significant pattern is largely captured by the LENS ensemble mean (Fig. 6c), indicating a substantial role for external forcing in driving the positive SAM pattern. However, consistent with the jet variations seen in Fig. 4d, the forcing from the tropical Pacific SST also contributes to the positive SAM pattern and better captures some of the details in the observed SLP changes, for example, the observed increase in SLP to the south of New Zealand, and the deepened Amundsen Sea low in the southeastern Pacific (Fig. 6d). The summation of the experiments (Fig. 6b) reproduces the observed positive SAM pattern reasonably well, with major contributions from external forcing and internal Pacific SST variability, but similar to Fig. 4b there are mismatches with some locations of the statistically significant regions.

b. Preindustrial control

The results in section 3a suggest that during the satellite era, on top of the external forcing influence, internally driven variability from tropical Pacific SSTs also contributed to driving the SH midlatitude atmospheric circulation variability on decadal time scales. Since the impact of the external forcing has been widely documented (see introduction), here we further investigate the influence of intrinsic variability originating from tropical Pacific SSTs by analyzing the CESM1 PI control simulations.

The leading EOF of the low-pass-filtered near-global (40°S–60°N) SST from years 400–2200 of the PI control shows a typical negative IPO phase, indicating that

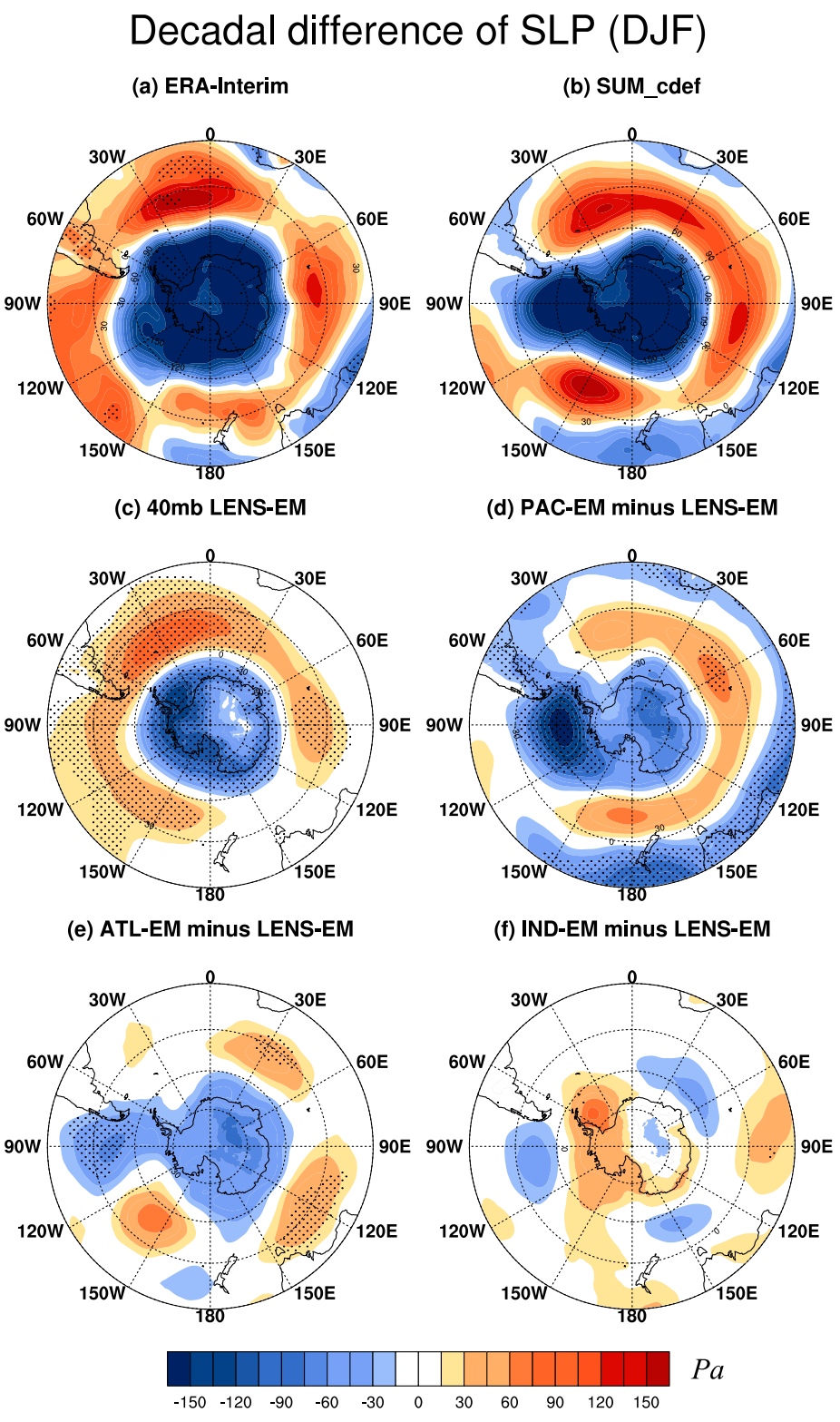

FIG. 6. The decadal difference between averaged P2 (1999–2013) and P1 (1979–98) for SLP. (a) ERA-Interim; (b) sum of (c)–(f); (c) LENS-EM; (d) Pacific pacemaker ensemble mean (PAC-EM) minus LENS-EM; (e) Atlantic pacemaker ensemble mean (ATL-EM) minus LENS-EM; and (f) Indian pacemaker ensemble mean (IND-EM) minus LENS-EM. Stippling indicates that differences are significant at the 95% level based on a *t* test.

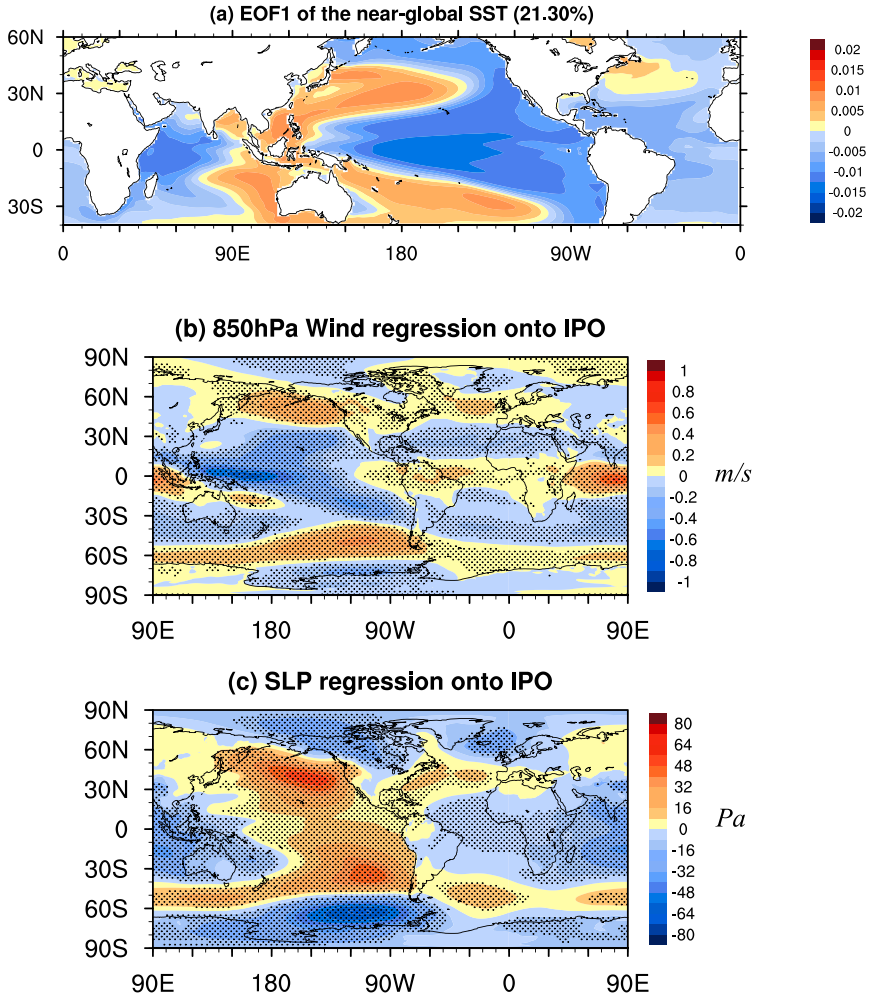

FIG. 7. (a) First EOF pattern calculated from low-pass-filtered (13-yr cutoff) near-global (40°S–60°N) SST from the preindustrial-control for years 400–2200. (b) Regression of 850-hPa *U* wind onto (a). (c) Regression of SLP onto (a). Stippling indicates that regressions are significant at the 95% level based on a *t* test.

the IPO is a dominant feature of the intrinsic variability in the climate system in the absence of external forcing (Fig. 7a). Regression of the 850-hPa zonal wind (Fig. 7b) onto the IPO time series (related PC1 of Fig. 7a; not shown) shows a zonally symmetric poleward migration of the eddy-driven jet in the South Atlantic and the Indian Ocean, as well as a strengthening in southeastern Pacific basin, which resembles our pacemaker results (Fig. 4d) and the uncoupled simulation results in Schneider et al. (2015) over the satellite era. The SLP regression (Fig. 7c) displays a positive SAM-like pattern (negative values at high latitudes) in the South Atlantic and Indian Ocean basins, combined with a deepened Amundsen Sea low, consistent with the decadal difference result for the observations and pacemaker experiments shown in Fig. 6, as well as previous research suggesting an impact of the IPO on Antarctic climate variability in this region (Meehl et al. 2016). This confirms the links among the IPO, SAM and the SH eddy-driven jet when examined over multiple samples and without the presence of external forcing.

c. *Extended IPO composite analysis*

To further examine the connections between IPO and SH extratropical circulation change, an extended IPO composite analysis (negative periods 1944–77 and 1999–2012, minus positive periods 1920–43 and 1978–98) is conducted for the length of the Pacific pacemaker simulations. Averaging over these two IPO cycles, this longer period IPO composite shows a significant poleward jet shift of around 1° latitude over the Indian Ocean basin and a strengthening of the jet in the southeastern Pacific (Fig. 8a), along with a positive SAM-like

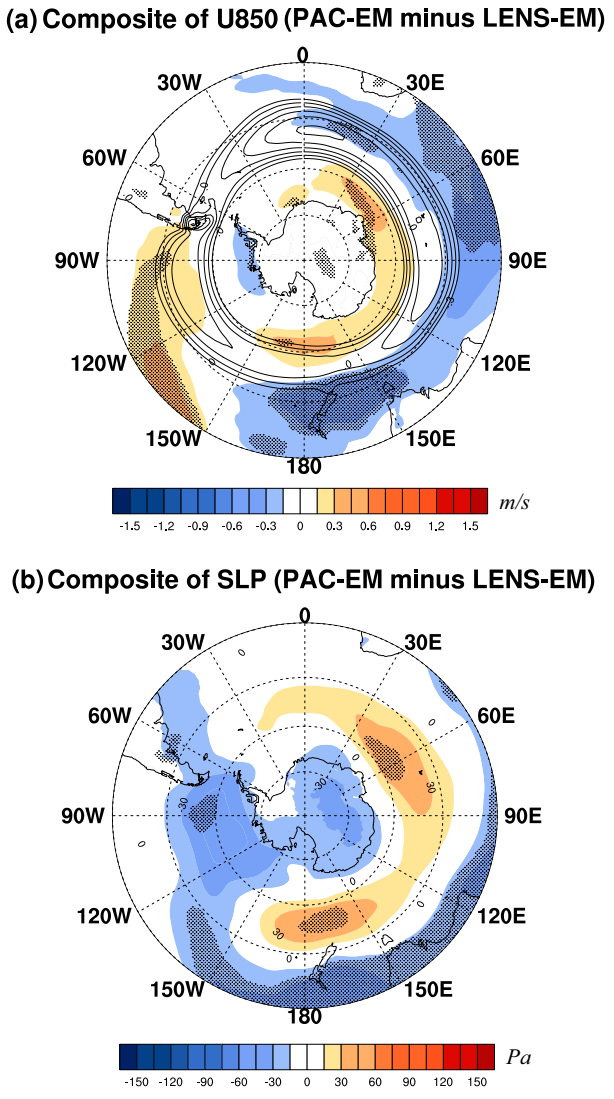

FIG. 8. The composite (colors) of (a) 850-hPa zonal wind and (b) SLP between negative IPO (1944–77, 1999–2012) and positive IPO (1921–43, 1978–98), from the Pacific pacemaker ensemble mean (PAC-EM) minus LENS-EM. Contours in (a) show the climatological midlatitude jet from 1921 to 2013 with an interval of 1 m s^{-1}. Stippling indicates that differences are significant at the 95% level based on a *t* test.

pattern and a deepened ASL (Fig. 8b), although with a weaker magnitude compared to Fig. 4d. Furthermore, in the extended IPO composite, the jet shift also occurs at a much higher latitude (around 55°S) compared to the reanalysis and recent decadal differences (about 50°S), as seen in Fig. 4d.

In summary, the results from this more extended multidecadal IPO composite analysis lend support to the previous analyses of the IPO teleconnection to the eddy-driven jet; namely, that the IPO is a key contributor to decadal variability of the SH extratropical atmospheric circulation.

4. Physical mechanism

Now, we turn to the question of how external forcing and tropical Pacific decadal variability affect the midlatitude jet displacement. Since the transient eddy–mean flow interactions are essential in eddy-driven jet development and maintenance (section 2c), previous studies have used this approach to explain the midlatitude atmospheric circulation change under global warming, ozone depletion, and its response to ENSO forcing (Lu et al. 2008; Hendon et al. 2014). For instance, according to Lu et al. (2008), the intensified upper-level meridional temperature gradient caused by increased GHGs can accelerate the phase speed of the transient eddies in the high latitudes. Then, the equatorward-propagating faster transient eddies break at a higher latitude around the equatorward side of the eddy-driven jet when they encounter the critical latitudes where the increased phase speed equals the background zonal wind speed. As a result, the eddy momentum flux convergence (EMFC) and divergence (EMFD) zones would shift poleward, and westerly winds would strengthen on the poleward flank of the climatological eddy-driven jet. In other words, global warming increases the transient eddy phase speed, which starts the eddy–mean flow feedback that leads to the poleward jet migration and the eddy-driven circulation change. Similarly, Butler et al. (2010) employed an idealized model and found that the SH polar stratospheric cooling caused by ozone depletion would induce the poleward shift of eddy momentum and heat fluxes, resulting in a poleward shift of the eddy-driven jet around 60°S. The EMFC responds to El Niño events in the opposite sense: during El Niño events, as the tropical eastern Pacific warms and the tropical–subtropical temperature gradient increases, the subtropical jet strengthens and shifts equatorward via thermal wind balance at the edge of the descending branch of the Hadley cell. The intensified subtropical jet draws the critical latitudes equatorward for waves of all speeds, which drags the whole eddy-driven meridional circulation equatorward, resulting in a negative phase of the SAM (Seager et al. 2003; Chen et al. 2008; Lu et al. 2008; Lim et al. 2019). However, few studies have investigated the response of the transient eddies and eddy-induced circulation to tropical Pacific SST variation over the decadal time scales.

First, we calculate the decadal difference of the upper-level EMFC as a function of angular phase speed (multiplied by Earth's radius) and latitude following Chen and Held (2007) and Chen et al. (2008). The

observed climatological EMFC (solid contours in Fig. 9a) is located at midlatitudes (40°–65°S) and induces the westerly jet. The climatological EMFD (dashed contours in Fig. 9a) belt is located in the subtropics as well as the polar region, with the subtropical EMFD terminating near the critical latitudes around 20°–25°S, where the phase speed equals the background zonal-mean zonal wind speed.

The decadal difference of the transient EMFC displays a dipole structure in the middle latitudes, with enhanced EMFC (red colors at 55°–65°S) on the poleward side of the climatological convergence belt and increased EMFD (blue colors at 40°–50°S) on its equatorward flank for eastward-propagating eddies. This indicates a poleward migration of the eddy-induced momentum convergence and divergence, resulting in a poleward movement of the zonal-mean zonal wind (the thick magenta compared to navy lines in Fig. 9a) by ~1° of latitude. The poleward migration of EMFC and the midlatitude jet is related to the steepened meridional temperature gradient around 50°S (Fig. 9b), with strengthened baroclinicity providing more energy for transient eddy generations as well as westerly strengthening on the poleward flank of the climatological jet. In the subtropics, the EMFD anomaly is in the same location as the climatological EMFD, and the subtropical wave-breaking latitude has barely changed in the two periods. The EMFC anomalies (the decrease of climatological EMFD) at 0°–20°S suggest that there is less eddy breaking in the deeper tropics due to the weakened zonal winds for speeds smaller than 15 $m\,s^{-1}$.

The contributions of external forcing and tropical Pacific SST are examined using LENS and Pacific pacemaker simulations. The zonal-mean temperature anomaly induced by external forcing (Fig. 9d) exhibits an overall warming in the middle and low latitudes as well as a cooling in the South Pole in the upper level, leading to a sharp meridional gradient at about 45°S; the increased meridional temperature gradient is also found in the middle troposphere (800–300 hPa). These would lead to an enhanced baroclinicity and more transient waves produced at higher latitudes; as a result, the climatological EMFC experiences a significant poleward migration at 55°–60°S (Fig. 9c), leading to jet intensification on its poleward flank (similar to Fig. 4c, polar region jet strengthening), thus inducing a poleward shift of the zonal-mean zonal wind by around 1° latitude. This result is in accordance with Fig. 10 of Lu et al. (2008) and with Butler et al. (2010) as discussed above, suggesting that the external forcing (including ozone depletion and global warming) can partly explain the observed zonal-mean jet migration. In the subtropics, there is not much response in either EMFD or zonal-mean zonal wind to the external forcing, suggesting there are other factors beyond anthropogenic forcing that drive the slight poleward shift of the zonal wind at 20°S in observation (Fig. 9a).

When the tropical Pacific SST is combined with the external forcing influence in the Pacific pacemaker simulation (Fig. 9e), the decadal difference of the zonal-mean zonal wind better matches the observations in the extratropics. Under this combined impact, a stronger EMFC (EMFD) anomaly at 60°S (45°S) is formed, with a slight increase of transient wave speed to 45 $m\,s^{-1}$. This appears to be associated with the meridional temperature structure induced by external forcing and negative IPO, with the latter warming the subtropics and increasing the meridional temperature gradient between the subtropics and the middle latitudes. With faster speed eddies generated and confined in the higher latitudes, eddies would break down at a higher latitude on the equatorward flank of the eddy-driven jet, resulting in a poleward shift of the eddy-driven jet. On the other hand, comparisons between Figs. 9e and 9c suggest that the influence of negative IPO on the zonal wind can be also found in the subtropics. The negative IPO, with reduced tropical–subtropical meridional temperature gradient and an expanded Hadley cell circulation, induces a slight deceleration of the subtropical jet around 20°S and a poleward displacement of the subtropical jet and wave-breaking critical latitude by ~0.3° of latitude through the EMFC anomaly (P2 − P1; orange color at ~25°S in Fig. 9e) on the equatorward side of the subtropical jet and EMFD anomaly on its poleward side. The midlatitude EMFD anomaly and the high-latitude EMFC anomaly combined induce a positive SAM circulation (Vallis et al. 2004), which further validates the Fig. 6d result. This subtropical EMFC anomaly and the slight shift of the wave-breaking critical latitude (at around 15°S) induced by negative IPO generally resemble the observation, although there are some disparities in terms of the magnitude and central locations of EMFC/EMFD anomaly, indicating either that there are other factors playing the opposite role as negative IPO in driving the positive SAM or that the model has uncertainties reproducing the reanalysis.

On top of the negative IPO-induced subtropical warming, the upper-level anomalous EMFC (dark red at ~60°S) with westerly acceleration (magenta line exceeds the black line to the right) in Fig. 9e would induce equatorward flow (due to the Coriolis force; see Fig. 9f), while the anomalous EMFD (dark blue at ~45°S) with easterly acceleration would induce a poleward flow (Hendon et al. 2014; Lim and Hendon 2015). Due to mass conservation, a downward tendency and a narrow adiabatic warming anomaly around

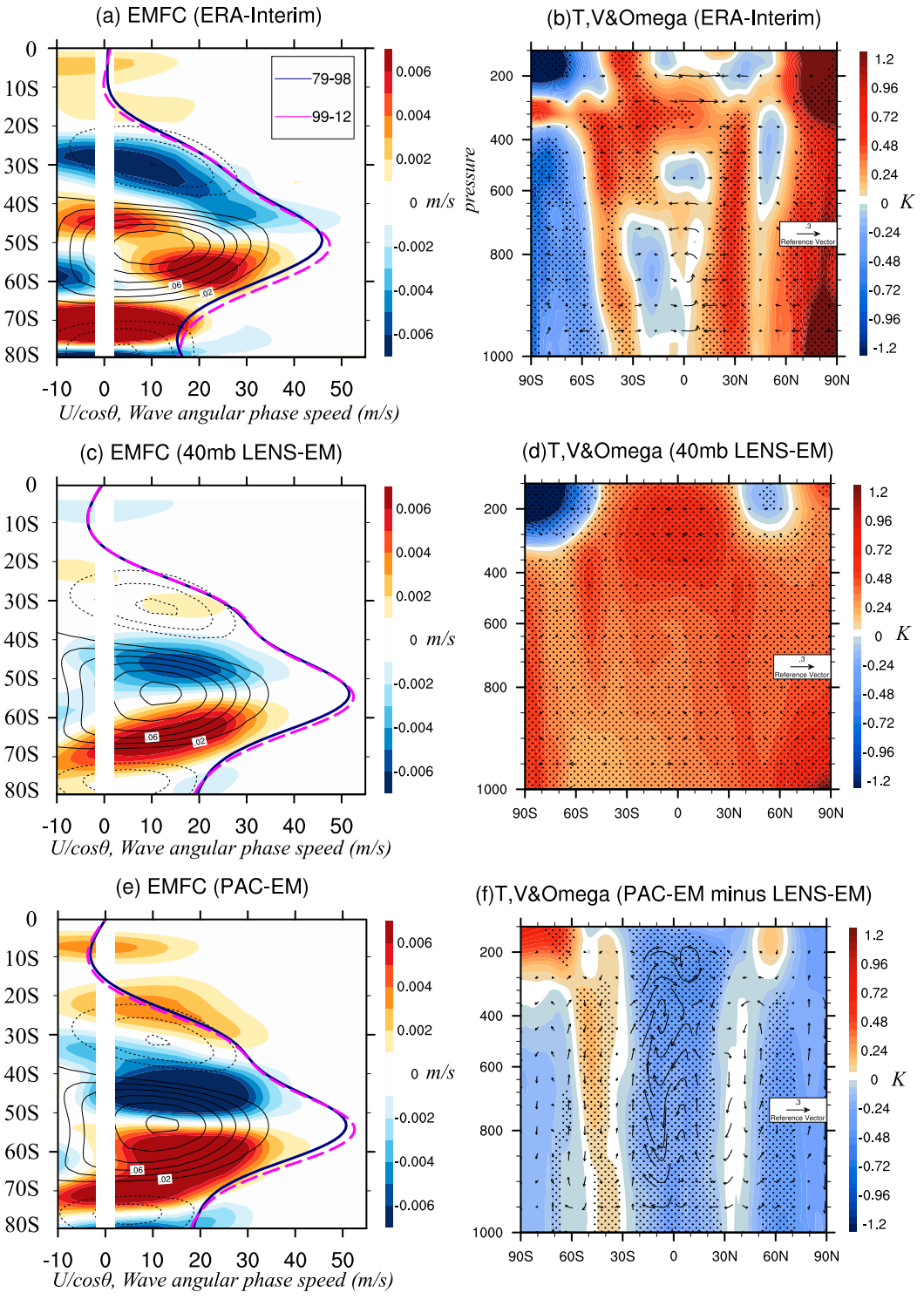

FIG. 9. (left) Cospectra of transient eddy momentum flux convergence at 200 hPa in DJF, as a function of wave angular phase speed (multiplied by Earth's radius) and latitude for (a) ERA-Interim, (c) LENS-EM, and (f) PAC-EM (note that LENS is not removed in this case). The contours are climatological-mean values over P1 (1979–98), with dashed (solid) contours indicating the transient eddy momentum flux divergence (convergence). The colored shading shows the decadal difference (1999–2013 minus 1979–98). The solid navy curve is the zonal-mean zonal wind (divided by $\cos\varphi$, where φ is latitude) averaging over P1. The dashed magenta curve is averaged over P2. (right) Decadal difference (P2 − P1) of temperature (color shading) and meridional and vertical velocity (v and omega, respectively; vectors) for (b) ERA-Interim, (d) LENS-EM, and (f) PAC-EM minus LENS-EM. Stippling indicates that differences are significant at the 95% level based on a t test.

50°–55°S would result as seen in the middle troposphere of Fig. 9f. This adiabatic warming would further strengthen the mid-to-high-latitude meridional temperature gradient, which encourages more eddy generation in the high latitudes, forming a positive feedback between the barotropic (wave breaking) and baroclinic processes (wave generation), and leading to a more persistent ''poleward shifted'' eddy-driven jet and positive SAM (Barnes et al. 2010; Nie et al. 2014).

Note that here we focus on a zonal-mean perspective, not only because the EMFC cospectra calculation requires longitudinal cyclicity, but also because the jet shift is largely zonally symmetric in austral summer (Fig. 4a). However, earlier studies demonstrated that anomalies in the activity of equivalent barotropic Rossby wave trains emanating from the tropical eastern Indian and western Pacific Oceans and propagating to the South Pacific could amplify the SAM response to tropical SST forcing (Lim et al. 2016a; Adames and Wallace 2017; Lim et al. 2019). Figure 4a also shows that the midlatitude circulation change is not entirely zonally symmetric, as in the South Pacific Ocean it is dominated by a jet intensification rather than a poleward shift. Thus, the metric using zonal-mean zonal wind could underestimate the poleward displacement of the main body of the eddy-driven jet.

The poleward displacement of the critical latitude in response to negative IPO is consistent with several previous studies. For example, Tandon et al. (2013) conducted a series of idealized thermal forcing experiments and found that with idealized global warming (their Fig. 2d), the midlatitude meridional temperature gradient increases and the eddy-driven jet shifts poleward; moreover in their Fig. 2g, with the subtropical warming anomaly, the Hadley cell expands and the eddy-driven jet also moves poleward (their Fig. 2h), which partly mimics the response to the negative IPO pattern in observations. Similarly, Mantsis et al. (2017) also suggested that the subtropics shifted poleward with an expansion of the Hadley cell during the early 2000s. In contrast to other studies that focused on the GHG influence, Mantsis et al. (2017) stressed the impact of tropical Pacific SST on the widening, analogous to our arguments that in response to the negative IPO, an expansion of the Hadley cell and a poleward migration of the eddy-driven jet would be induced.

5. Discussion and conclusions

A methodology using the CESM LENS and pacemaker experiments has been applied to isolate the external forcing signals from the internal tropical SST influence on decadal shifts of the SH eddy-driven jet during austral summer. The pacemaker experiments are nudged separately to observed SSTs in three tropical basins: the tropical central and eastern Pacific Ocean basin, the tropical Indian and western Pacific Ocean basin, and the tropical and North Atlantic Ocean basin. Our work extends on previous studies that focused on the contribution of external forcing to trends in the SH extratropical circulation over the twentieth century, by zeroing in on the decadal differences across the shorter satellite era. In addition, the response to tropical SSTs is further examined for each tropical basin individually. The decadal difference result shows a zonally symmetric poleward shift in the eddy-driven jet, with external forcing and internal variability originating from tropical Pacific SST playing comparably dominant roles, and the tropical and North Atlantic SST and Indian Ocean SST appearing to make a weak and sometimes offsetting contribution. Consistent patterns are found for longer composites over the historical period and preindustrial control simulations.

A dynamical mechanism of external forcing and tropical Pacific SSTAs inducing eddy-driven circulation variations was examined. We found that the poleward shift of the transient eddy momentum flux convergence could fundamentally explain the poleward migration of the eddy-driven jet from a zonal symmetric perspective. Under the external forcing influence, the midlatitude EMFC shows a significant poleward migration around 55°S, leading to the southward migration of the eddy-driven jet by ~1° of latitude. In addition to the external forcing component, the importance of tropical Pacific SST has also been demonstrated. During negative IPO, the meridional temperature gradient between the subtropics and the middle latitudes is further increased, resulting in faster speed eddies generated in the higher latitudes, thus leading to the poleward migration of EMFC and eddy-driven jet. In addition, the subtropical EMFD and associated subtropical wave-breaking critical latitude displaces poleward for slower eddies during negative IPO, pushing the midlatitude EMFC and eddy-driven jet farther poleward. On top of this tropical–extratropical association, the ''poleward shifted'' eddy momentum flux convergence/divergence would lead to a midlatitude warming anomaly (around 55°S; Fig. 9d), also steepening the mid-to-high meridional SST gradient and leading to a positive feedback to generate more baroclinic transient eddies, accelerating the westerlies at higher latitudes. Besides, there is also evidence suggesting a feedback of zonal wind and SAM onto the EMFC; for instance, Barnes et al. (2010) found that when the jet is at high latitudes, the wave-breaking

critical latitude would move poleward and eddies would break at higher latitudes, which would in turn maintain the positive phase. Via this extratropical eddy–mean flow interaction, the poleward jet movement would be more persistent (Barnes et al. 2010; Nie et al. 2014). The mechanism of external forcing and negative IPO influence on the midlatitude circulation through the enhanced meridional temperature gradient is similar to the impact of global warming on the midlatitude jet in some previous studies (Chen et al. 2008; Lu et al. 2008). However, there is some weak contribution from the poleward shifted subtropical critical latitude in response to negative IPO, although the subtropical EMFD barely moves, which is different from the La Niña events established by Lu et al. (2008). Here we identify the importance of EMFC analysis in understanding eddy-driven circulation changes to decadal Pacific SST variability.

However, there are some questions that remain to be addressed. First, we note that the eddy-driven jet in the South Pacific region responds somewhat differently to the southern Atlantic and southern Indian Ocean basins. In both the observations and response to tropical Pacific SSTs (Figs. 4d and 8a), the jet experiences an intensification in the South Pacific with a deepened Amundsen Sea low (ASL), compared to the poleward movement in the South Atlantic and southern Indian Ocean basins. While previous studies have suggested that the negative IPO could largely explain the deepened ASL in the austral cool seasons, through an anomalous stationary Rossby wave response, similar analysis for the austral summer season leads to a weakened ASL, opposite to that observed (Meehl et al. 2016; Clem et al. 2019). Therefore, further work is needed to understand the zonally asymmetric jet strengthening in the South Pacific basin. Second, an interdependence between the tropical basins exists that makes it difficult to isolate each basin's contribution in a linear way (Cai et al. 2019). For instance, due to the air–sea coupling and interbasin coupling in the pacemaker runs, the tropical Pacific SSTA forcing can promote a response in other tropical basins that can then force their own teleconnection to midlatitudes. In fact, teleconnections between three tropical basins have been widely documented (Ashok et al. 2004; Li et al. 2016). Therefore, a linear summation of each coupled component (external forcing and three tropical ocean forcings) could therefore overestimate (or underestimate) the influence of tropical SSTs on extratropical circulation change, as discussed in section 2b. Third, the mechanisms by which tropical Indian and Atlantic Ocean SSTs influence the SH midlatitude circulation require further exploration but were limited by data availability and model deficiencies in simulating the interbasin SST interactions (Cai et al. 2019) in this study. It should also be noted that the estimation of the external forcing influence on the EMFC poleward shift and eddy-driven jet migration could be somewhat member-dependent in magnitude. To best estimate the externally forced signal and to be comparable with previous work using LENS (Solomon and Polvani 2016; Chung et al. 2019; Holland et al. 2019; Zhang et al. 2019), we used all 40 LENS members. Finally, model and SST errors may also play a role. For example, there is a strong link between clouds and the eddy-driven jet (Ceppi et al. 2012; Ceppi and Hartmann 2015) and there are known errors in CMIP5 class models in simulating clouds over the Southern Ocean (Kay et al. 2016).

Our work highlights the combination of external forcing and tropical Pacific SSTs in driving the recent decadal variability of the SH summertime eddy-driven jet, and the physical processes associated with eddy–mean flow interactions through which this has occurred. These findings could have significant implications for decadal prediction of the Southern Hemisphere atmospheric circulation. For instance, the IPO appeared to transition into a positive phase around 2014–16 (Meehl et al. 2019b), which, along with ozone recovery, might potentially offset the impact of greenhouse gases in driving a poleward shift of the eddy-driven jet over the coming decade.

Acknowledgments. This work was supported by 1) the Australian Research Council Centre of Excellence for Climate Extremes (Grant CE170100023); 2) the Regional and Global Model Analysis (RGMA) component of the Earth and Environmental System Modeling Program of the U.S. Department of Energy's Office of Biological and Environmental Research (BER) Cooperative Agreement DE-FC02-97ER62402; and 3) the National Center for Atmospheric Research, which is a major facility sponsored by the National Science Foundation under Cooperative Agreement 1852977. Most figures were created using NCAR Command Language (NCL) version 6.5.0 on National Computational Infrastructure (NCI), which is supported by the Australian Government. We thank Harry Hendon from the Australian Bureau of Meteorology for helpful comments, and the NCAR and UCAR Computational and Information Systems Lab (CISL) for technical support. Computing resources (doi:10.5065/D6RX99HX) were provided by the Climate Simulation Laboratory at NCAR's Computational and Information Systems Laboratory, sponsored by the National Science Foundation and other agencies.

REFERENCES

Adames, Á. F., and J. M. Wallace, 2017: On the tropical atmospheric signature of El Niño. *J. Atmos. Sci.*, **74**, 1923–1939, https://doi.org/10.1175/JAS-D-16-0309.1.

Arblaster, J. M., and G. A. Meehl, 2006: Contributions of external forcings to southern annular mode trends. *J. Climate*, **19**, 2896–2905, https://doi.org/10.1175/JCLI3774.1.

Ashok, K., Z. Guan, N. Saji, and T. Yamagata, 2004: Individual and combined influences of ENSO and the Indian Ocean dipole on the Indian summer monsoon. *J. Climate*, **17**, 3141–3155, https://doi.org/10.1175/1520-0442(2004)017<3141:IACIOE>2.0.CO;2.

Barnes, E. A., D. L. Hartmann, D. M. Frierson, and J. Kidston, 2010: Effect of latitude on the persistence of eddy-driven jets. *Geophys. Res. Lett.*, **37**, L11804, https://doi.org/10.1029/2010GL043199.

Butler, A. H., D. W. J. Thompson, and R. Heikes, 2010: The steady-state atmospheric circulation response to climate change–like thermal forcings in a simple general circulation model. *J. Climate*, **23**, 3474–3496, https://doi.org/10.1175/2010JCLI3228.1.

Cai, W., and Coauthors, 2019: Pantropical climate interactions. *Science*, **363**, eaav4236, https://doi.org/10.1126/science.aav4236.

Ceppi, P., and D. L. Hartmann, 2015: Connections between clouds, radiation, and midlatitude dynamics: A review. *Curr. Climate Change Rep.*, **1**, 94–102, https://doi.org/10.1007/s40641-015-0010-x.

——, Y.-T. Hwang, D. M. W. Frierson, and D. L. Hartmann, 2012: Southern Hemisphere jet latitude biases in CMIP5 models linked to shortwave cloud forcing. *Geophys. Res. Lett.*, **39**, L19708, https://doi.org/10.1029/2012GL053115.

Chen, G., and I. M. Held, 2007: Phase speed spectra and the recent poleward shift of Southern Hemisphere surface westerlies. *Geophys. Res. Lett.*, **34**, L21805, https://doi.org/10.1029/2007GL031200.

——, J. Lu, and D. M. Frierson, 2008: Phase speed spectra and the latitude of surface westerlies: Interannual variability and global warming trend. *J. Climate*, **21**, 5942–5959, https://doi.org/10.1175/2008JCLI2306.1.

Chipperfield, M. P., and Coauthors, 2017: Detecting recovery of the stratospheric ozone layer. *Nature*, **549**, 211–218, https://doi.org/10.1038/nature23681.

Chung, E.-S., A. Timmermann, B. J. Soden, K.-J. Ha, L. Shi, and V. O. John, 2019: Reconciling opposing Walker circulation trends in observations and model projections. *Nat. Climate Change*, **9**, 405–412, https://doi.org/10.1038/s41558-019-0446-4.

Cionni, I., and Coauthors, 2011: Ozone database in support of CMIP5 simulations: Results and corresponding radiative forcing. *Atmos. Chem. Phys.*, **11**, 11 267–11 292, https://doi.org/10.5194/acp-11-11267-2011.

Clem, K. R., B. R. Lintner, A. J. Broccoli, and J. R. Miller, 2019: Role of the South Pacific convergence zone in West Antarctic decadal climate variability. *Geophys. Res. Lett.*, **46**, 6900–6909, https://doi.org/10.1029/2019GL082108.

Dee, D. P., and Coauthors, 2011: The ERA-Interim reanalysis: Configuration and performance of the data assimilation system. *Quart. J. Roy. Meteor. Soc.*, **137**, 553–597, https://doi.org/10.1002/qj.828.

Deser, C., and A. S. Phillips, 2009: Atmospheric circulation trends, 1950–2000: The relative roles of sea surface temperature forcing and direct atmospheric radiative forcing. *J. Climate*, **22**, 396–413, https://doi.org/10.1175/2008JCLI2453.1.

England, M. H., and Coauthors, 2014: Recent intensification of wind-driven circulation in the Pacific and the ongoing warming hiatus. *Nat. Climate Change*, **4**, 222–227, https://doi.org/10.1038/nclimate2106.

Eyring, V., and Coauthors, 2013: Long-term ozone changes and associated climate impacts in CMIP5 simulations. *J. Geophys. Res. Atmos.*, **118**, 5029–5060, https://doi.org/10.1002/JGRD.50316.

Fogt, R. L., D. H. Bromwich, and K. M. Hines, 2011: Understanding the SAM influence on the South Pacific ENSO teleconnection. *Climate Dyn.*, **36**, 1555–1576, https://doi.org/10.1007/s00382-010-0905-0.

Gong, D., and S. Wang, 1999: Definition of Antarctic Oscillation index. *Geophys. Res. Lett.*, **26**, 459–462, https://doi.org/10.1029/1999GL900003.

Gong, T., S. B. Feldstein, and D. Luo, 2013: A simple GCM study on the relationship between ENSO and the southern annular mode. *J. Atmos. Sci.*, **70**, 1821–1832, https://doi.org/10.1175/JAS-D-12-0161.1.

Hendon, H. H., E.-P. Lim, and H. Nguyen, 2014: Seasonal variations of subtropical precipitation associated with the southern annular mode. *J. Climate*, **27**, 3446–3460, https://doi.org/10.1175/JCLI-D-13-00550.1.

Holland, P. R., T. J. Bracegirdle, P. Dutrieux, A. Jenkins, and E. J. Steig, 2019: West Antarctic ice loss influenced by internal climate variability and anthropogenic forcing. *Nat. Geosci.*, **12**, 718–724, https://doi.org/10.1038/s41561-019-0420-9.

Hurrell, J. W., and Coauthors, 2013: The Community Earth System Model: A framework for collaborative research. *Bull. Amer. Meteor. Soc.*, **94**, 1339–1360, https://doi.org/10.1175/BAMS-D-12-00121.1.

Karpechko, A. Y., D. Maraun, and V. Eyring, 2013: Improving Antarctic total ozone projections by a process-oriented multiple diagnostic ensemble regression. *J. Atmos. Sci.*, **70**, 3959–3976, https://doi.org/10.1175/JAS-D-13-071.1.

Kay, J. E., and Coauthors, 2015: The Community Earth System Model (CESM) Large Ensemble Project: A community resource for studying climate change in the presence of internal climate variability. *Bull. Amer. Meteor. Soc.*, **96**, 1333–1349, https://doi.org/10.1175/BAMS-D-13-00255.1.

——, A. Y., C. Wall, V. Yettella, B. Medeiros, C. Hannay, P. Caldwell, and C. Bitz, 2016: Global climate impacts of fixing the Southern Ocean shortwave radiation bias in the Community Earth System Model (CESM). *J. Climate*, **29**, 4617–4636, https://doi.org/10.1175/JCLI-D-15-0358.1.

Kosaka, Y., and S.-P. Xie, 2013: Recent global-warming hiatus tied to equatorial Pacific surface cooling. *Nature*, **501**, 403–407, https://doi.org/10.1038/nature12534.

Kushner, P. J., I. M. Held, and T. L. Delworth, 2001: Southern Hemisphere atmospheric circulation response to global warming. *J. Climate*, **14**, 2238–2249, https://doi.org/10.1175/1520-0442(2001)014<0001:SHACRT>2.0.CO;2.

Lee, S., and S. B. Feldstein, 2013: Detecting ozone- and greenhouse gas–driven wind trends with observational data. *Science*, **339**, 563–567, https://doi.org/10.1126/science.1225154.

L'Heureux, M. L., and D. W. J. Thompson, 2006: Observed relationships between the El Niño–Southern Oscillation and the extratropical zonal-mean circulation. *J. Climate*, **19**, 276–287, https://doi.org/10.1175/JCLI3617.1.

Li, X., E. P. Gerber, D. M. Holland, and C. Yoo, 2015: A Rossby wave bridge from the tropical Atlantic to West Antarctica. *J. Climate*, **28**, 2256–2273, https://doi.org/10.1175/JCLI-D-14-00450.1.

——, S.-P. Xie, S. T. Gille, and C. Yoo, 2016: Atlantic-induced pan-tropical climate change over the past three decades. *Nat. Climate Change*, **6**, 275–279, https://doi.org/10.1038/nclimate2840.

Lim, E.-P., and H. H. Hendon, 2015: Understanding and predicting the strong southern annular mode and its impact on the record wet east Australian spring 2010. *Climate Dyn.*, **44**, 2807–2824, https://doi.org/10.1007/s00382-014-2400-5.

——, ——, J. M. Arblaster, C. Chung, A. F. Moise, P. Hope, G. Young, and M. Zhao, 2016a: Interaction of the recent 50 year SST trend and La Niña 2010: Amplification of the southern annular mode and Australian springtime rainfall. *Climate Dyn.*, **47**, 2273–2291, https://doi.org/10.1007/s00382-015-2963-9.

——, ——, ——, F. Delage, H. Nguyen, S. K. Min, and M. C. Wheeler, 2016b: The impact of the Southern Annular Mode on future changes in Southern Hemisphere rainfall. *Geophys. Res. Lett.*, **43**, 7160–7167, https://doi.org/10.1002/2016GL069453.

——, ——, P. Hope, C. Chung, F. Delage, and M. J. McPhaden, 2019: Continuation of tropical Pacific Ocean temperature trend may weaken extreme El Niño and its linkage to the Southern Annular Mode. *Sci. Rep.*, **9**, 17044, https://doi.org/10.1038/s41598-019-53371-3.

Lu, J., G. Chen, and D. M. Frierson, 2008: Response of the zonal mean atmospheric circulation to El Niño versus global warming. *J. Climate*, **21**, 5835–5851, https://doi.org/10.1175/2008JCLI2200.1.

Luo, J.-J., G. Wang, and D. Dommenget, 2018: May common model biases reduce CMIP5's ability to simulate the recent Pacific La Niña-like cooling? *Climate Dyn.*, **50**, 1335–1351, https://doi.org/10.1007/s00382-017-3688-8.

Mantsis, D. F., S. Sherwood, R. Allen, and L. Shi, 2017: Natural variations of tropical width and recent trends. *Geophys. Res. Lett.*, **44**, 3825–3832, https://doi.org/10.1002/2016GL072097.

Marsh, D. R., M. J. Mills, D. E. Kinnison, J.-F. Lamarque, N. Calvo, and L. M. Polvani, 2013: Climate change from 1850 to 2005 simulated in CESM1(WACCM). *J. Climate*, **26**, 7372–7391, https://doi.org/10.1175/JCLI-D-12-00558.1.

McGregor, S., A. Timmermann, M. F. Stuecker, M. H. England, M. Merrifield, F.-F. Jin, and Y. Chikamoto, 2014: Recent Walker circulation strengthening and Pacific cooling amplified by Atlantic warming. *Nat. Climate Change*, **4**, 888–892, https://doi.org/10.1038/nclimate2330.

——, M. F. Stuecker, J. B. Kajtar, M. H. England, and M. Collins, 2018: Model tropical Atlantic biases underpin diminished Pacific decadal variability. *Nat. Climate Change*, **8**, 493–498, https://doi.org/10.1038/s41558-018-0163-4.

Meehl, G. A., J. M. Arblaster, C. M. Bitz, C. T. Y. Chung, and H. Teng, 2016: Antarctic sea-ice expansion between 2000 and 2014 driven by tropical Pacific decadal climate variability. *Nat. Geosci.*, **9**, 590–595, https://doi.org/10.1038/ngeo2751.

——, and Coauthors, 2019a: Mutually interactive decadal-timescale processes connecting the tropical Atlantic and Pacific. *2019 Fall Meeting*, San Francisco, CA, Amer. Geophys. Union, Abstract OS23A-01.

——, J. M. Arblaster, C. T. Chung, M. M. Holland, A. DuVivier, L. Thompson, D. Yang, and C. M. Bitz, 2019b: Sustained ocean changes contributed to sudden Antarctic sea ice retreat in late 2016. *Nat. Commun.*, **10**, 14, https://doi.org/10.1038/s41467-018-07865-9.

Moss, R. H., and Coauthors, 2010: The next generation of scenarios for climate change research and assessment. *Nature*, **463**, 747–756, https://doi.org/10.1038/nature08823.

Nie, Y., Y. Zhang, G. Chen, X. Q. Yang, and D. A. Burrows, 2014: Quantifying barotropic and baroclinic eddy feedbacks in the persistence of the Southern Annular Mode. *Geophys. Res. Lett.*, **41**, 8636–8644, https://doi.org/10.1002/2014GL062210.

Polvani, L. M., D. W. Waugh, G. J. Correa, and S.-W. Son, 2011: Stratospheric ozone depletion: The main driver of twentieth-century atmospheric circulation changes in the Southern Hemisphere. *J. Climate*, **24**, 795–812, https://doi.org/10.1175/2010JCLI3772.1.

Purich, A., and M. H. England, 2019: Tropical teleconnections to Antarctic sea ice during austral spring 2016 in coupled pacemaker experiments. *Geophys. Res. Lett.*, **46**, 6848–6858, https://doi.org/10.1029/2019GL082671.

——, T. Cowan, S.-K. Min, and W. Cai, 2013: Autumn precipitation trends over Southern Hemisphere midlatitudes as simulated by CMIP5 models. *J. Climate*, **26**, 8341–8356, https://doi.org/10.1175/JCLI-D-13-00007.1.

——, W. Cai, M. H. England, and T. Cowan, 2016: Evidence for link between modelled trends in Antarctic sea ice and underestimated westerly wind changes. *Nat. Commun.*, **7**, 10409, https://doi.org/10.1038/ncomms10409.

Randel, W. J., and I. M. Held, 1991: Phase speed spectra of transient eddy fluxes and critical layer absorption. *J. Atmos. Sci.*, **48**, 688–697, https://doi.org/10.1175/1520-0469(1991)048<0688:PSSOTE>2.0.CO;2.

Rayner, N., D. E. Parker, E. Horton, C. K. Folland, L. V. Alexander, D. Rowell, E. Kent, and A. Kaplan, 2003: Global analyses of sea surface temperature, sea ice, and night marine air temperature since the late nineteenth century. *J. Geophys. Res.*, **108**, 4407, https://doi.org/10.1029/2002JD002670..

Schneider, D. P., and C. Deser, 2017: Tropically driven and externally forced patterns of Antarctic sea ice change: Reconciling observed and modeled trends. *Climate Dyn.*, **50**, 4599–4618, https://doi.org/10.1007/S00382-017-3893-5.

——, ——, and T. Fan, 2015: Comparing the impacts of tropical SST variability and polar stratospheric ozone loss on the Southern Ocean westerly winds. *J. Climate*, **28**, 9350–9372, https://doi.org/10.1175/JCLI-D-15-0090.1.

Seager, R., N. Harnik, Y. Kushnir, W. Robinson, and J. Miller, 2003: Mechanisms of hemispherically symmetric climate variability. *J. Climate*, **16**, 2960–2978, https://doi.org/10.1175/1520-0442(2003)016<2960:MOHSCV>2.0.CO;2.

Simpson, I. R., C. Deser, K. A. McKinnon, and E. A. Barnes, 2018: Modeled and observed multidecadal variability in the North Atlantic jet stream and its connection to sea surface temperatures. *J. Climate*, **31**, 8313–8338, https://doi.org/10.1175/JCLI-D-18-0168.1.

Smith, T. M., R. W. Reynolds, T. C. Peterson, and J. Lawrimore, 2008: Improvements to NOAA's historical merged land–ocean surface temperature analysis (1880–2006). *J. Climate*, **21**, 2283–2296, https://doi.org/10.1175/2007JCLI2100.1.

Solomon, A., and L. M. Polvani, 2016: Highly significant responses to anthropogenic forcings of the midlatitude jet in the Southern Hemisphere. *J. Climate*, **29**, 3463–3470, https://doi.org/10.1175/JCLI-D-16-0034.1.

Swart, N. C., and J. C. Fyfe, 2012: Observed and simulated changes in the Southern Hemisphere surface westerly wind-stress. *Geophys. Res. Lett.*, **39**, L16711, https://doi.org/10.1029/2012GL052810.

——, ——, N. Gillett, and G. J. Marshall, 2015: Comparing trends in the southern annular mode and surface westerly jet. *J. Climate*, **28**, 8840–8859, https://doi.org/10.1175/JCLI-D-15-0334.1.

Tandon, N. F., E. P. Gerber, A. H. Sobel, and L. M. Polvani, 2013: Understanding Hadley cell expansion versus contraction: Insights from simplified models and implications for recent

observations. *J. Climate*, **26**, 4304–4321, https://doi.org/10.1175/JCLI-D-12-00598.1.

Taylor, K. E., R. J. Stouffer, and G. A. Meehl, 2012: An overview of CMIP5 and the experiment design. *Bull. Amer. Meteor. Soc.*, **93**, 485–498, https://doi.org/10.1175/BAMS-D-11-00094.1.

Thompson, D. W., and S. Solomon, 2002: Interpretation of recent Southern Hemisphere climate change. *Science*, **296**, 895–899, https://doi.org/10.1126/science.1069270.

Vallis, G. K., 2006: *Atmospheric and Oceanic Fluid Dynamics: Fundamentals and Large-Scale Circulation*. Cambridge University Press, 745 pp.

——, E. P. Gerber, P. J. Kushner, and B. A. Cash, 2004: A mechanism and simple dynamical model of the North Atlantic Oscillation and annular modes. *J. Atmos. Sci.*, **61**, 264–280, https://doi.org/10.1175/1520-0469(2004)061<0264:AMASDM>2.0.CO;2.

Wang, C., L. Zhang, S.-K. Lee, L. Wu, and C. R. Mechoso, 2014: A global perspective on CMIP5 climate model biases. *Nat. Climate Change*, **4**, 201–205, https://doi.org/10.1038/nclimate2118.

Wang, G., H. H. Hendon, J. M. Arblaster, E.-P. Lim, S. Abhik, and P. van Rensch, 2019: Compounding tropical and stratospheric forcing of the record low Antarctic sea-ice in 2016. *Nat. Commun.*, **10**, 13, https://doi.org/10.1038/s41467-018-07689-7.

Yin, J. H., 2005: A consistent poleward shift of the storm tracks in simulations of 21st century climate. *Geophys. Res. Lett.*, **32**, L18701, https://doi.org/10.1029/2005GL023684.

Yu, J.-Y., H. Paek, E. S. Saltzman, and T. Lee, 2015: The early 1990s change in ENSO–PSA–SAM relationships and its impact on Southern Hemisphere climate. *J. Climate*, **28**, 9393–9408, https://doi.org/10.1175/JCLI-D-15-0335.1.

Zhang, L., W. Han, K. B. Karnauskas, G. A. Meehl, A. Hu, N. Rosenbloom, and T. Shinoda, 2019: Indian Ocean warming trend reduces Pacific warming response to anthropogenic greenhouse gases: An interbasin thermostat mechanism. *Geophys. Res. Lett.*, **46**, 10 882–10 890, https://doi.org/10.1029/2019GL084088.